Hindawi
Advances in Condensed Matter Physics
Volume 2022, Article ID 6002025, 8 pages
https://doi.org/10.1155/2022/6002025

Research Article

Dielectric and Impedance Spectroscopic Investigation of (3-Nitrophenol) -2,4,6-Triamino-1,3,5- Triazine: An Organic Crystalline Material

N. Kanagathara,[1] **S. Sankar**,[2] **L. Saravanan**,[1] **V. Natarajan**,[3] **and S. Elangovan**[4]

[1]*Department of Physics, Saveetha School of Engineering, Saveetha Institute of Medical and Technical Sciences, Thandalam, Chennai 602 105, India*
[2]*Department of Physics, Indira Institute of Engineering and Technology, V.G.R. Nagar, Pandur, Thiruvallur 631 203, India*
[3]*Department of Physics, Rajalakshmi Institute of Technology, Kuthambakkam, Chennai 600 124, India*
[4]*Department of Physics, College of Natural and Computational Science, Wollega University, Nekemte, Ethiopia*

Correspondence should be addressed to S. Elangovan; elangovan.physics@rediffmail.com

Received 13 June 2022; Accepted 3 August 2022; Published 5 September 2022

Academic Editor: Junjie Li

This article presents the investigation of dielectric and impedance spectroscopic properties of an organic product of 3-nitrophenol -2,4,6-tri amino-1,3,5- triazine (3NPTAT) single crystal, synthesized from melamine and m-nitrophenol. Comprehensive dielectric studies and charge transportation properties of the grown 3NPTAT crystal are given. The dielectric characteristics of the specimen were carried out in the frequency range of 50 Hz and 5 MHz at different temperatures, namely, 313 K, 333 K, 353 K, and 373 K. From the spectra, it was observed that the slowdown occurs at low temperatures, and the hopping mechanism takes place based on localized charge carriers. The impedance spectroscopic results indicate that there is a single relaxation process that occurs at high frequencies. The variation detected in the material properties of 3NPTAT corresponding to the temperature and frequency has been discussed in detail.

1. Introduction

Single crystals with low dielectric constant, high electro-optic coefficient and ideal reaction rate, and significant thermal stability play a crucial role in producing efficient crystalline materials that might be used in optical data storage, communication, and optoelectronic systems [1–5]. Dielectric spectroscopic studies will be used to determine the electric field distribution in the formed crystal. The frequency and temperature-dependent dielectric characteristics of the produced material reveal the 3NPTAT single crystal's applicability for a variety of applications. The dielectric characteristics of formed crystals were investigated at frequencies ranging from 50 Hz to 5 MHz.

The dielectric behavior of a substance is based on its electrical properties. Materials with a high dielectric constant and low dielectric losses are said to be more suitable for electronic applications. The permittivity of nonconductive materials was previously measured using a dielectric spectroscopic approach [6–11]. Dielectric characteristics also provide useful information regarding materials and design parameters for a variety of applications. Complex impedance spectroscopic examination of frequency-dependent electrical and dielectric properties of materials provides significant information about their electrical microstructure [12–14]. The effect of solvent on material properties using impedance has been discussed by S. Khera and P. Chand in their investigation of ZnO [15]. The complex characteristics such as dielectric permittivity, electrical modulus, impedance, and admittance in the complex plane were shown to explain the whole electrical topography of material by creating a graph between real and imaginary parts in the dielectric spectrum. Dielectric spectroscopic investigations of organic single crystals with desired NLO properties have already been reported by many researchers [16–20].

The dielectric and impedance behavior of 3-nitrophenol -2,4,6-tri amino-1,3,5-triazine (3NPTAT) is investigated in this study as a continuation of our research effort in organic NLO materials. We discovered that 3NPTAT has considerable optical transparency throughout the visible spectrum, implying that the dielectric susceptibility is related to precise ordering in the dielectric dipole density. To demonstrate the effect of grain and grain boundaries on the electrical properties of a produced material, we used a combined analysis of modulus and impedance spectroscopy investigation. The authors planned the study to include dielectric measurements as well as conductivity and impedance measurements on the formed crystal.

2. Experimental

The slow evaporation approach was used to make a single crystal of 3-nitrophenol -2,4,6-tri amino-1,3,5-triazine (3NPTAT) using an equimolar ratio of melamine and 3-nitrophenol. Melamine was dissolved in distilled water and gently heated before adding an aqueous solution of 3-nitrophenol to the hot melamine solution. The mixture was then thoroughly agitated for 6 hours at 70°C to obtain a homogeneous solution. To obtain the purity of the salt, a recrystallization process was carried out. Tiny and transparent single crystals of 3NPTAT were produced for 25–30 days [21]. The schematic of the synthesis procedure is given in the flow chart in Figure 1, and the growth mechanism of the 3NPTAT single crystal is shown in Figure 2.

The dielectric characterization of the synthesized compound is carried out using a suitably cut and polished pellet made of 3NPTAT crystal. Dielectric studies of 3NPTAT crystal were performed at different temperatures and frequencies in the range of 313 K–373 K and 50 Hz–5 MHz, respectively, using the HIOKI model 3532–50 LCR HITESTER impedance analyzer. The polished sides of the crystal pellet have been coated with silver paste and air-dried (for good ohmic contact) to make parallel electrodes.

3. Results and Discussion

3.1. Dielectric Analysis. Permittivity ε^*, conductivity $\sigma^*(x)$, and permeability $\mu^*(x)$ are inherent electrical properties of materials that are of great interest in both fundamental and application-oriented research [22]. Based on temperature variations, charge transport, the molecule, collective dipolar fluctuations, and polarisation effects at inner phase boundaries were studied. This article reports the impedance and modulus spectroscopic investigations in detail as a continuation of our prior work on the dielectric constant and dielectric loss as a function of frequency.

The resistive property of the grown crystals can be obtained from dielectric studies. The measured dielectric properties are primarily related to the electro-optical properties of an optical single crystal [23]. It further gives insight into the charge transportation properties and charge storage capabilities of the dielectric material. The electronic industries require materials with a low dielectric constant that can be used as a dielectric interlayer during microelectronic device fabrication [24, 25]. Figures 3 and 4 represent the variation of dielectric constant and dielectric loss as a function of frequency, respectively, at different temperatures, namely, 313K, 333K, 353K, and 373 K. Earlier, Sangeetha et al. have previously reported a virtually consistent reduction in dielectric constant with increasing frequency, from 50 Hz to 5 MHz (2014). Figure 4 shows that the decreasing trend in dielectric loss with increasing frequency suggests that the optical quality of the formed 3NPTAT crystal is good with few imperfections, making it appropriate for photonics, laser, and electro-optic device manufacturing. The fact that the dielectric constant and dielectric loss are reduced at higher frequencies indicates that the formed crystal contains a small number of electrically active flaws, which is important in NLO applications [26].

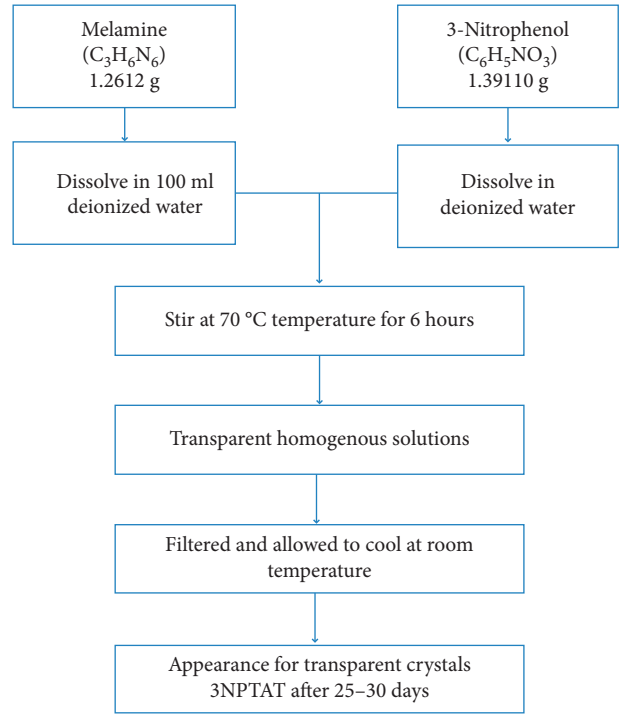

Figure 1: Synthesis flow chart of the 3NPTAT single crystal.

3.2. Frequency Dependence of Real and Imaginary Parts of Dielectric Constant. Figures 5 and 6 show the frequency-dependent real (ε') and imaginary (ε") parts of the dielectric constant at various temperatures, including 313 K, 333 K, 353 K, and 373 K. The ability to retain electrical energy is the real component of dielectric, whereas the ability to lose electrical energy owing to fluctuations in an applied electric field is the imaginary part. Excellent insulating properties are found in materials with a high dielectric constant and low dielectric loss (tan δ). Figure 6 shows that at low frequencies, the obtained high dielectric constant (ε r) values are due to interfacial or space charge polarisations. It can also be seen that at all temperatures, the real part of the dielectric constant (ε') decreases with increasing frequency and reaches a maximum value at high frequencies.

The increase in conductivity of the material at high frequencies is caused by a decreasing trend in the imaginary part of the dielectric constant, as shown in Figure 7, which is

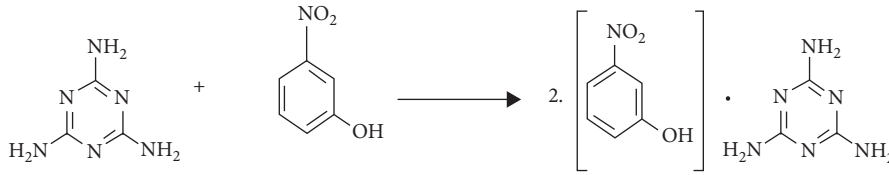

Figure 2: Reaction mechanism of the grown crystal of 3NPTAT.

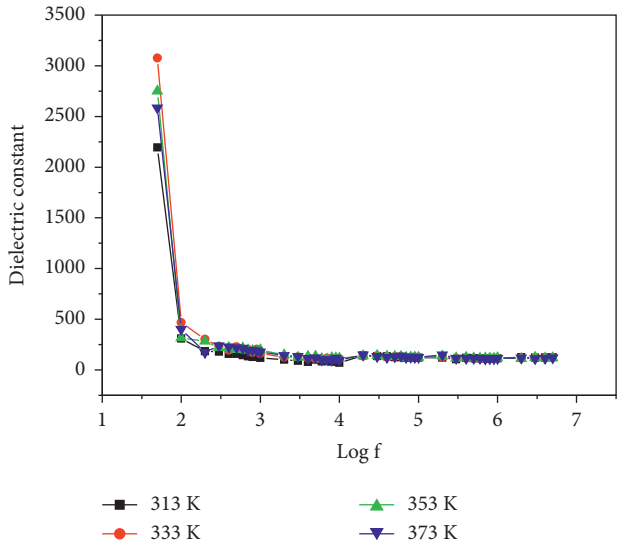

Figure 3: Dielectric constant vs log F of 3NPTAT.

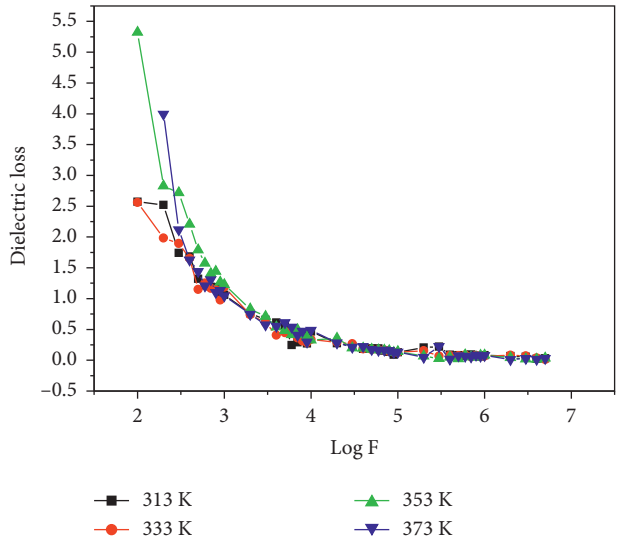

Figure 4: Dielectric loss vs log F of 3NPTAT.

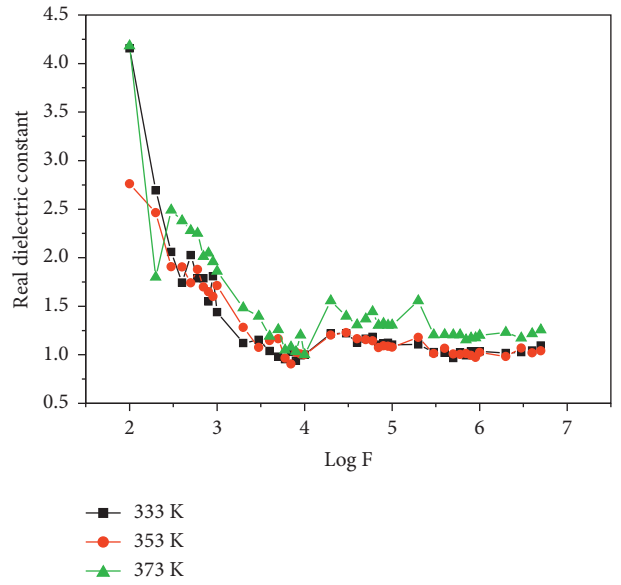

Figure 5: Real dielectric constant (ε) vs log F.

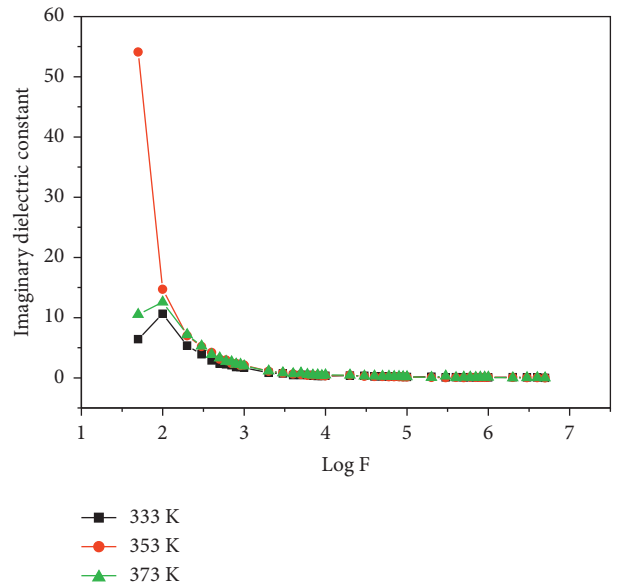

Figure 6: Imaginary dielectric constant (ε") vs log F.

similar to the earlier report [27]. At low frequencies, the grain boundary effect would be more pronounced. The effect of dielectric polarisation is caused by electrons/holes hopping between both the positive and negative surface defect centers in the grain boundary region at low frequencies. At 373 K, the imaginary dielectric constant is high, indicating that the imaginary part of the dielectric constant (ε') grows as temperature rises, although the real dielectric constant (ε') is high at 353 K. At high temperatures, larger grains form, lowering the energy barrier and accelerating atom diffusion to another grain in a single crystal. According to the findings, all types of polarisation (electronic, ionic, orientation, and space charge) play a significant role, but electronic polarisation is the most important [28].

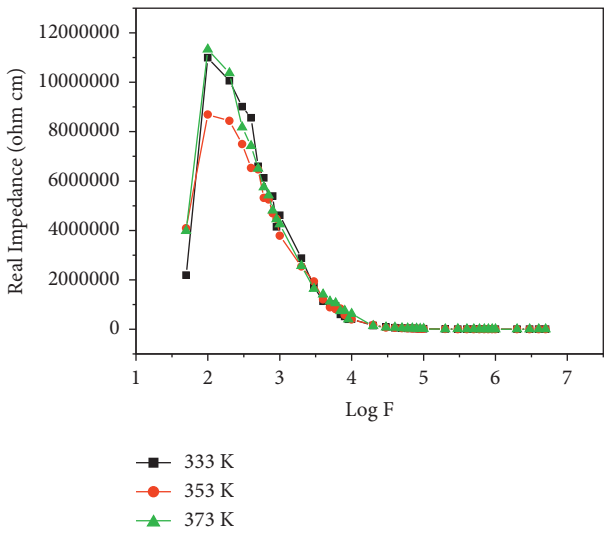

Figure 7: Real impedance vs log F.

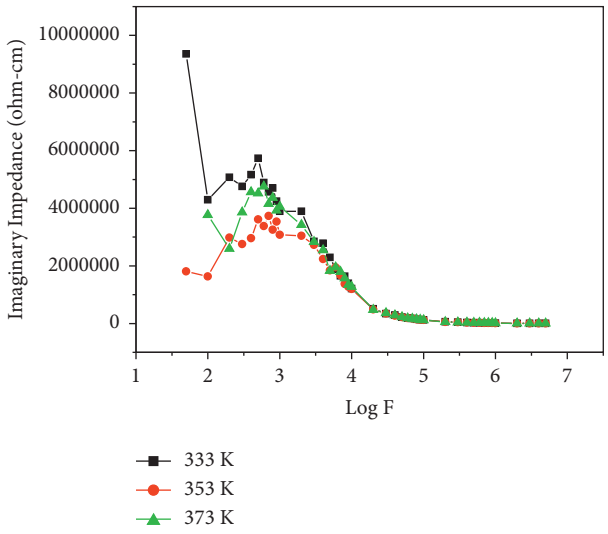

Figure 8: Imaginary impedance vs log F.

3.3. Complex Impedance Spectroscopic Studies. Complex impedance spectroscopy techniques can be employed to circumvent the restrictions in frequency-dependent dielectric constant and dielectric loss [29–34]. To understand the dielectric behavior and electrical conductivity of materials, the Cole–Cole plot is commonly used in impedance spectroscopic studies to determine the variation among various parameters such as permittivity, impedance, electric modulus, and tangent loss as a function of frequency [35]. The microstructure level of the material can be determined via a complex impedance spectroscopy investigation. It aids in determining how charge transfer occurs in the material as well as how much it relaxes. The response at high frequency is attributable to grains, while the response at low frequency is due to grain boundaries, according to impedance data from the dielectric system plotted in the complex plane.

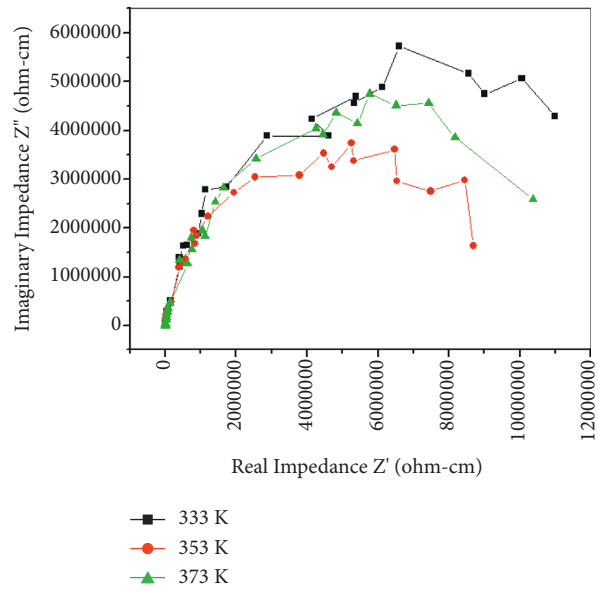

Figure 9: Real impedance vs imaginary impedance.

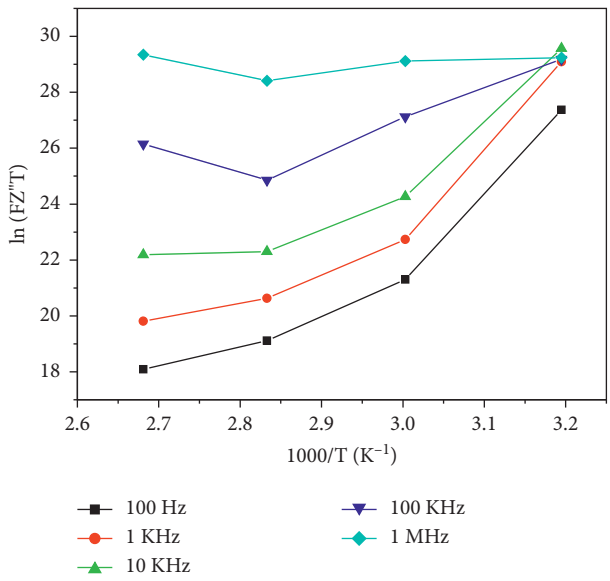

Figure 10: ln (FZ"T) vs 1000/T (K^{-1}).

Figures 7 and 8 depict the fluctuation in real and imaginary impedance as a function of frequency at various temperatures, including 313 K, 333 K, 353 K, and 373 K.

The complex impedance spectra of 3NPTAT at various temperatures are shown in Figure 9. At all temperatures, all of the samples have a single semicircle shape, as shown in Figure 9. The linear representation of bulk resistivity is given by the semicircle on the real axis. The semicircle represents a grain boundary effect for 3NPTAT at 373 K, with the decrease in impedance value due to increased grain size or grain growth [32, 33]. Figure 10 shows how to compute the activation energy for the thermodynamic system Z. Table 1 shows the activation energy derived from different

Table 1: Activation energy (E_a) obtained from impedance values.

Frequency	Activation energy (eV)	Pre-exponential factor (s^{-1})	R^2 value	Standard deviation
100 Hz	83.33	8.952	0.969	0.403
1 KHz	76.04	4.907	0.955	0.453
10 KHz	54.41	4.336	0.816	0.707
100 KHz	98.97	8.781	0.995	0.193
1 MHz	18.69	22.152	0.827	0.263
2 MHz	8.334	3.755	0.9329	0.987
3 MHz	28.51	1.599	0.9547	0.278
4 MHz	34.04	1.9615	0.7921	1.039
5 MHz	36.01	1.9199	0.7981	5.579

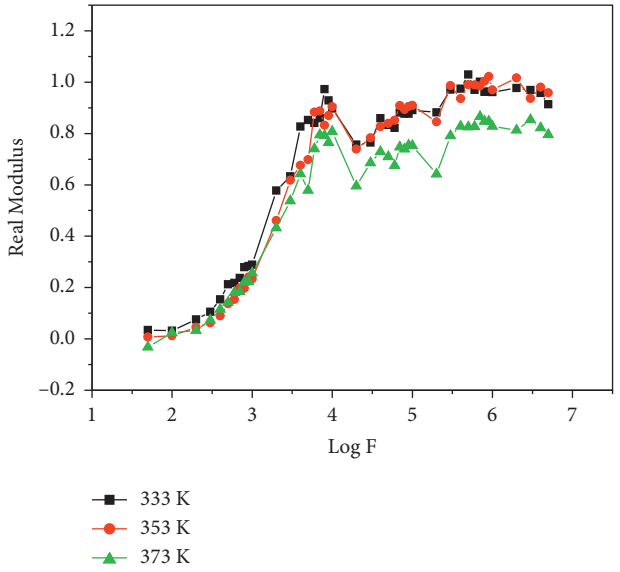

Figure 11: Real modulus vs log F.

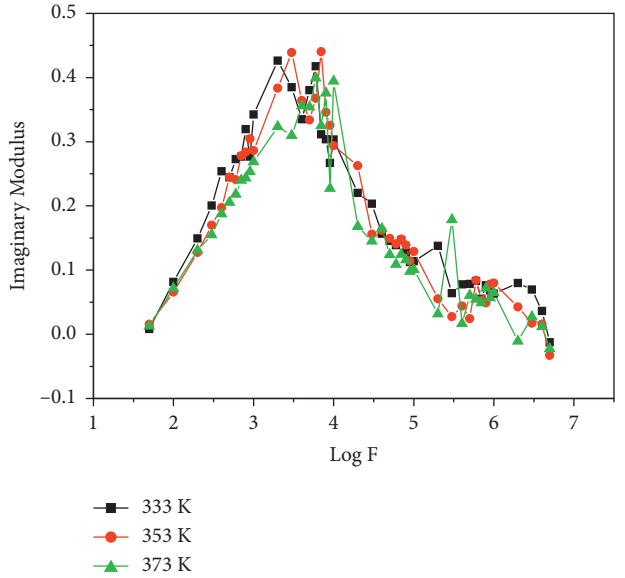

Figure 12: Imaginary modulus vs log F.

frequencies based on the imaginary impedance of single-crystal 3NPTAT. Table 1 shows that the activation energy value for a particular frequency above 1 MHz is in the range of 0.02–0.03 eV, whereas for lower frequencies below 1 MHz, the value is greater (0.04–0.07 eV). At low frequencies, charge carriers are thought to travel a great distance and are restricted to a potential well at high frequencies [27, 30].

3.4. Dielectric Modulus Studies. Sinclair and West explained that to understand the dielectric properties of a given material, both complex impedance and modulus investigations are used [31]. The grain boundary effect and the conduction mechanism were distinguished using a complex dielectric modulus analysis. The real and imaginary plots of frequency-dependent electric modulus by altering the measurement temperature are shown in Figures 11 and 12. M' increases with frequency, reaches a peak at 0.45 rad/s, and then steadily falls at high frequencies, indicating the semiconductor property. Because of the short-range mobility of ion charges and their confinement in the potential well, the asymmetric real electric modulus shifts towards higher frequency regions [27]. Furthermore, at low frequencies, the real component of the dielectric modulus is low, implying that electrode polarisation is minimal.

When compared to dielectric loss, the imaginary portion of the dielectric modulus is utilized to characterize the relaxation nature of the materials. The obtained modulus plot shows that electrical relaxation occurs in the produced crystal. At room temperature, the complex moduli of the M' and M'' series draw semicircles in the complex plane. The two depressed semicircular graphs for the 3NPTAT crystal recorded at 373 K are shown in Figure 13. The linear spikes in the low-frequency band of the Nyquist plot in Figure 13 indicate a supercapacitive nature. This happens because the ions in the electrolyte intercalate and pass through the electrode [36–38].

The conductivity relaxation's peak breadth indicates that the single relaxation time is related to the Debye process. Figure 14 shows a conductivity relaxation peak in the M" vs log (f) curve, which shows a minor shift towards higher frequency with increasing 3NPTAT concentration. The shorter relaxation time ($\tau = 1/\text{fmax}$) and greater polaronic hopping rate in the concentration of 3NPTAT are related to the rise in peak frequency. The charts plainly illustrate that the arcs' centers do not correspond to the real axis. The first semicircle is due to

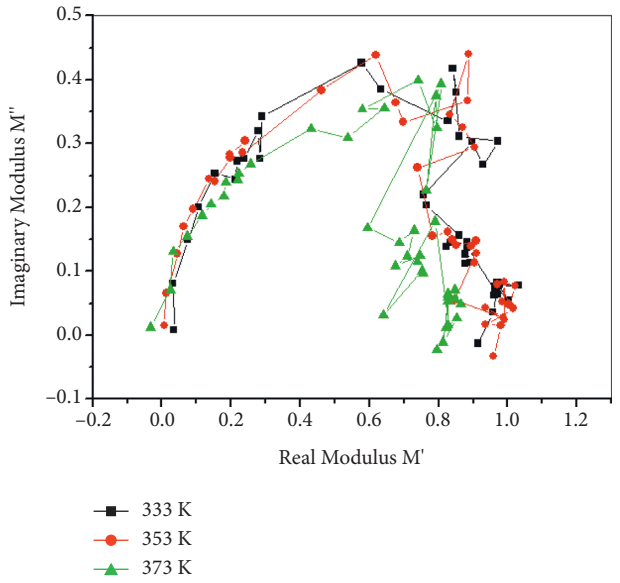

Figure 13: Real modulus vs imaginary modulus.

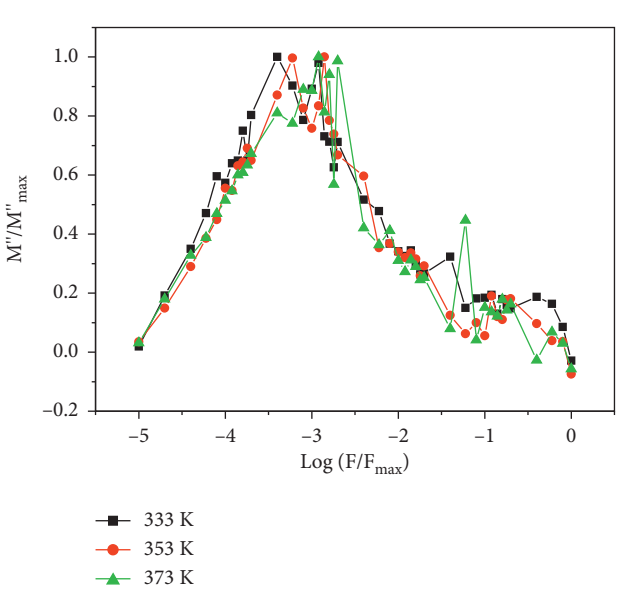

Figure 14: Normalized curve of M'/M''max versus log (F/Fmax).

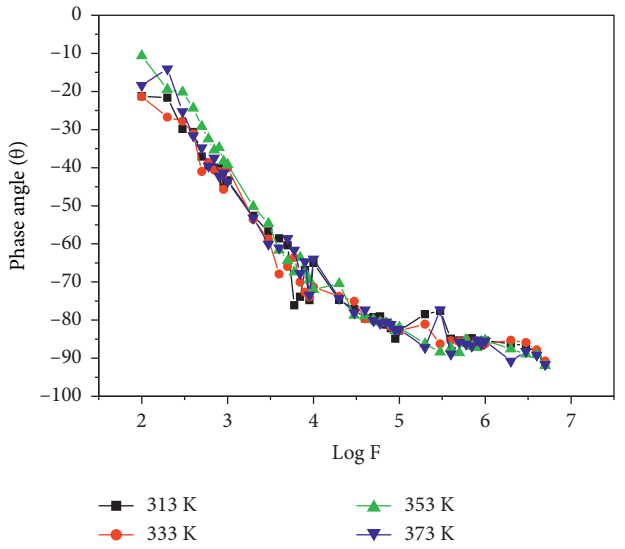

Figure 15: Phase angle vs log F.

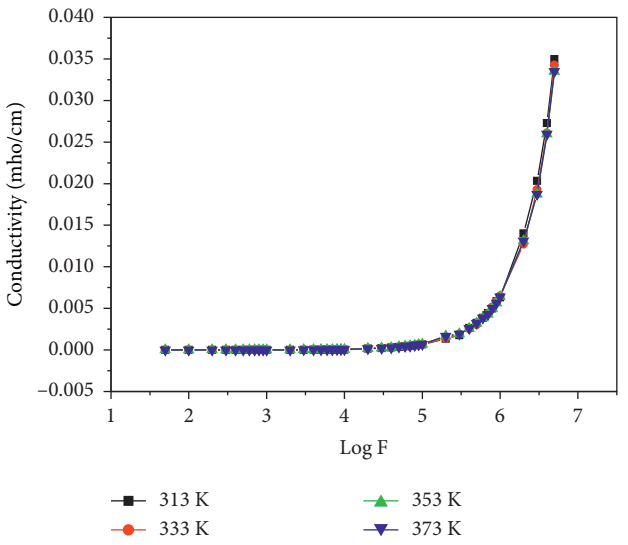

Figure 16: Conductivity vs log F.

the grain boundary effect at lower frequencies, although this impact is not visible in the impedance plot or Nyquist plot at higher frequencies.

A Bode plot is a graph that shows the amplitude and phase of a transfer function in a linear system on a logarithmic scale. Figure 15 depicts the fluctuation of the Bode phase angle concerning applied angular frequency (Bode plots). In an EIS Bode plot, the crystal has nearly the same morphology across the whole frequency range and for all temperature measurements. For all the samples examined at different temperatures, a higher phase angle close to 90° was seen at low frequency (a feature of an ideal capacitor). This corresponds to the cell's capacitive functionality. The appearance of a single peak over the whole frequency range shows the presence of grain effects for the generated single-crystal 3NPTAT. The dielectric characteristics of the materials are altered by grain effects. We can adjust the dielectric characteristics by changing the grain size of dielectric materials by varying parameters such as growth temperature, stoichiometric composition, postsintering temperature, and so on.

The ac conductivity is determined using the following formula:

$$\sigma = \frac{A}{2\pi f C d}, \tag{1}$$

where C is the capacitance, d is the crystal thickness, A is the crystal area of cross-section, and f is the applied field frequency. Figure 16 shows the frequency dependence of electrical conductivity at various temperatures. It signifies that as frequency rises, conductivity rises as well, following Jonscher's universal power law.

$$\sigma_{ac} = \sigma_o + \sigma_\omega. \quad (2)$$

σ_o is the frequency-independent conductivity; σ_ω is the frequency-dependent conductivity, which is expressed as follows:

$$\sigma(\omega) = A\omega^s \; where \; 0 \le s \le 1. \quad (3)$$

Here, ω is the angular frequency of the applied ac field.

$$A = \frac{\pi N^2 e^2}{6K_B T(2a)}. \quad (4)$$

Conductivity is essentially nonexistent up to 3 MHz. Beyond 3 MHz, conductivity rises and yields a slope at hopping frequency, indicating that the formed 3NPTAT crystal is thermally active [39].

4. Conclusion

In the frequency range of 50 Hz to 5 MHz, the dielectric and charge transport properties of the synthesized nonlinear optical material 3NPTAT single crystal were investigated at four different temperatures 313 K, 333 K, 353 K, and 373 K. The determined dielectric constant $'$ and dielectric loss $''$ showed decreasing trends with frequency elsewhere. The influence of the electric field on the dipoles explained the drop in ε'. At low frequencies, these dipole moments easily follow the direction of the alternating applied field, resulting in significant polarisation values, as shown by high values of ε'. However, at high frequencies, dipoles have difficulties following the field's direction, polarisation weakens, and constant dielectric ε' values fall. After analyzing the data, it was shown that charge transportation relaxation and hopping mechanisms occur at low temperatures with concentrated charge carriers. The results also show that the grain boundary effect causes a single relaxation process at a high frequency. The increase in modulus with frequency attains the maximum value again, and a decrease in modulus shows the semiconducting character. This trend also shows that the relaxation mechanism is dominated by dipole orientation relaxation under the influence of the electric field. The combination of impedance spectroscopy and modulus yields a lot of information on the electrical relaxation process in the microstructure of materials. At higher frequencies, the activation energy is determined to be 8–36 eV, which explains relaxation in the lower region, where charge carriers are stable and can travel long distances. 3NPTAT is activated at high temperatures according to the frequency-dependent electrical conductivity measurements, and the material exhibits a low dielectric loss and a high dielectric constant. As a result, possible dielectric relaxations, conduction mechanisms, and the electrical field effect were examined in the context of this formalism. According to the findings, the produced 3NPTAT single crystal acts as a perfect insulator and a superior dielectric material for high-frequency device applications.

Data Availability

The authors confirm that the data supporting the findings of this study are available within the article.

Conflicts of Interest

The authors declare that there are no conflicts of interest.

References

[1] R. Mesbeh, B. Hamdi, and R. Zouari, "Synthesis, crystal structure, physicochemical characterization, and dielectric properties of anew organic chloride salt, $(C_3H_7N_6)Cl{\cdot}0.5H_2O$," *Ionics*, vol. 25, no. 12, pp. 6147–6160, 2019.

[2] K. Kahouli, A. Kahouli, K. Khirouni, and S. Chaabouni, "Crystal structure, thermal studies, vibrational properties, atomic Hirshfeld surface, and electrical and dielectric studies of [C9H14N] 3BiCl6 single crystal," *Journal of Molecular Structure*, vol. 1199, Article ID 126944, 2020.

[3] K. Venkatesan, M. Kayalvizhi, L. Jothi, and G. Vasuki, "Growth, structural, optical, Z-scan and dielectric analysis of 2-Amino-4-methylpyridinium 2-chloro 4-nitro benzoate crystals for third order non-linear optical applications," *Journal of Molecular Structure*, vol. 1258, Article ID 132687, 2022.

[4] P. Lunkenheimer, S. Krohns, F. Gemander, W. W. Schmahl, and A. Loidl, "Dielectric characterization of a nonlinear optical material," *Materials Science Reports*, vol. 4, no. 1, Article ID 6020, 2014.

[5] D. Shalini, S. Kalainathan, N. Hema, R. Usha, and D. Jayalakshmi, "Synthesis, growth and broadband dielectriccharacterization of nonlinear optical single crystal: 4-methylpyridinium5-sulfosalicylate," *Materials Research Innovations*, vol. 23, no. 2, pp. 94–99, 2017.

[6] R. C. Kambale, P. A. Shaikh, C. H. Bhosale, K. Y. Rajpure, and Y. D. Kolekar, "Dielectric properties and complex impedance spectroscopy studies of mixed Ni–Co ferrites," *Smart Materials and Structures*, vol. 18, no. 8, Article ID 085014, 2009.

[7] D. Luo and H. S. Chen, "A new generalized fractional maxwell model of dielectric relaxation," *Chinese Journal of Physics*, vol. 55, no. 5, pp. 1998–2004, 2017.

[8] J. H. Joshi, D. K. Kanchan, M. J. Joshi, H. Jethva, and K. Parikh, "Dielectric relaxation, complex impedance and modulus spectroscopic studies of mix phase rod like cobalt sulfide nanoparticles," *Materials Research Bulletin*, vol. 93, pp. 63–73, 2017.

[9] C. Elissalde and J. Ravez, "Ferroelectric ceramics: defects and dielectric relaxations," *Journal of Materials Chemistry*, vol. 11, no. 8, pp. 1957–1967, 2001.

[10] G. Hefter and R. Buchner, "Dielectric relaxation spectroscopy: an old-but-new technique for the investigation of electrolyte solutions," *Pure and Applied Chemistry*, vol. 92, no. 10, pp. 101595–101609, 2020.

[11] S. Nowy, W. Ren, J. Wagner, J. A. Weber, and W. Brutting, "Impedance spectroscopy of organic hetero-layer OLEDs as a probe for charge carrier injection and device degradation," *SPIE Proceedings*, vol. 7415, 2009.

[12] V. Purohit, R. Padhee, and R. Choudhary, "Dielectric and impedance spectroscopy of Bi (Ca0. 5Ti0. 5) O3 ceramic," *Ceramics International*, vol. 44, no. 4, pp. 3993–3999, 2018.

[13] T. Arumanayagam and P. Murugakoothan, "Optical conductivity and dielectric response of an organic aminopyridine NLO single crystal," *Journal of Minerals and Materials Characterization and Engineering*, vol. 10, no. 13, pp. 1225–1231, 2011.

[14] S. Sadhasivam and N. P. Rajesh, "Optical, structural, thermal and dielectric spectroscopy characterizations of seeded melt grown 2- hydroxy biphenyl single crystal," *Spectrochimica*

Acta Part A: Molecular and Biomolecular Spectroscopy, vol. 130, pp. 263–269, 2014.

[15] S. Khera and P. Chand, "Influence of different solvents on the structural, optical, impedance and dielectric properties of ZnO nanoflakes," *Chinese Journal of Physics*, vol. 57, pp. 28–46, 2019.

[16] N. Kanagathara, N. G. Renganathan, M. K. Marchewka et al., "Growth and characterization of melaminium bis (trichloroacetate dihydrate)," *Spectrochimica Acta Part A: Molecular and Biomolecular Spectroscopy*, vol. 101, pp. 112–118, 2013.

[17] S. Boomadevi, H. P. Mittal, and R. Dhansekaran, "Synthesis, crystal growth and characterization of 3-methyl 4- nitropyridine 1-oxide (POM) single crystals," *Journal of Crystal Growth*, vol. 261, no. 1, pp. 55–62, 2004.

[18] B. D. Hatton, K. Landskron, W. J. Hunks et al., "Materials chemistry for low-k materials," *Materials Today*, vol. 9, no. 3, pp. 22–31, 2006.

[19] S. Goma, C. M. Padma, and C. K. Mahadevan, "Dielectric parameters of KDP single crystals added with urea," *Materials Letters*, vol. 60, no. 29-30, pp. 3701–3705, 2006.

[20] S. Karatas and A. Türüt, "The determination of interface state energy distribution of the H-terminated Zn/p-type Si Schottky diodes with high series resistance by the admittance spectroscopy," *Vacuum*, vol. 74, no. 1, pp. 45–53, 2004.

[21] V. Sangeetha, M. Govindarajan, N. Kanagathara, M. Marchewka, S. Gunasekaran, and G. Anbalagan, "Vibrational, DFT, thermal and dielectric studies on 3-nitrophenol-1, 3, 5-triazine-2, 4, 6-triamine (2/1)," *Spectrochimica Acta Part A: Molecular and Biomolecular Spectroscopy*, vol. 118, pp. 1025–1037, 2014.

[22] F. Chen and R. Balieu, "A state-of-the-art review of intrinsic and enhanced electrical properties of asphalt materials: theories, analyses and applications," *Materials and Design*, vol. 195, Article ID 109067, 2020.

[23] P. S. Aithal, H. Nagaraja, P. M. Rao, D. Avasthi, and A. Sarma, "Effect of high energy ion irradiation on electrical and optical properties of organic nonlinear optical crystals," *Vacuum*, vol. 48, pp. 991–994, 1997.

[24] M. Ben Bechir, K. Karoui, M. Tabellout, K. Guidara, and A. Ben Rhaiem, "Dielectric relaxation, modulus behaviour and thermodynamic properties in $[N(CH_3)_3H]_2ZnCl_4$]," *Phase Transitions*, vol. 91, no. 8, pp. 901–917, 2018.

[25] S. K. Bhattacharya and R. R. Tummala, "Integral passives for next generation of electronic packaging: application of epoxy/ceramic nanocomposites as integral capacitors," *Microelectronics Journal*, vol. 32, no. 1, pp. 11–19, 2001.

[26] V. Parol, A. N. Prabhu, M. A. Taher, S. R. G. Naraharisetty, N. K. Lokanath, and V. Upadhyaya, "A third-order nonlinear optical single crystal of 3, 4-dimethoxy-substituted chalcone derivative with high laser damage threshold value: a potential material for optical power limiting," *Journal of Materials Science: Materials in Electronics*, vol. 31, no. 12, pp. 9133–9150, 2020.

[27] S. Subramani, K. Narayanan, N. Viswanathan, and C. R. A. John Chelliah, "Broadband dielectric spectroscopic investigation of melaminium bis(trichloroacetate) dihydrate-a nonlinear optical single crystal," *Journal of Materials Science: Materials in Electronics*, vol. 32, no. 8, pp. 10778–10788, 2021.

[28] N. Kanagathara and G. Anbalagan, "Growth, optical and dielectric studies on pure and L- lysine doped KDP crystals," *International Journal of Optics*, vol. 2012, pp. 1–6, 2012.

[29] H. Mahamoud, B. Louati, F. Hlel, and K. Guidara, "Impedance spectroscopy study of Pb2P2O7 compound," *Ionics*, vol. 17, no. 3, pp. 223–228, 2011.

[30] C. R. A. John Chelliah and R. Swaminathan, "Improved optical absorption, enhanced morphological and electrochemical properties of pulsed laser deposited binary zinc and vanadium oxide thin films," *Journal of Materials Science: Materials in Electronics*, vol. 31, no. 10, pp. 7348–7358, 2020.

[31] D. C. Sinclair and A. R. West, "Impedance and modulus spectroscopy of semiconducting BaTiO3 showing positive temperature coefficient of resistance," *Journal of Applied Physics*, vol. 66, no. 8, pp. 3850–3856, 1989.

[32] B. Behera, P. Nayak, and R. N. P. Choudhary, "Study complex impedance spectroscopic properties of $LiBa_2Nb_5O_{15}$ ceramics," *Materials Chemistry and Physics*, vol. 106, no. 2-3, pp. 193–197, 2007.

[33] M. Belal Hossen and A. K. M. Akther Hossain, "Complex impedance and electric modulus studies of magnetic ceramic Ni0.27Cu0.10Zn0.63Fe2O4," *Journal of Advanced Ceramics*, vol. 4, no. 3, pp. 217–225, 2015.

[34] K. Kumari, A. Prasad, and K. Prasad, "Dielectric, impedance/modulus and conductivity studies on [Bi0.5(Na1-x Kx)0.5] 0.94Ba0.06TiO3, lead-free ceramics," *American Journal of Materials Science*, vol. 6, p. 1, 2016.

[35] J. G. Powles, "Cole-Cole plots as they should be," *Journal of Molecular Liquids*, vol. 56, pp. 35–47, 1993.

[36] P. Victor, S. Bhattacharyya, and S. B. Krupanidhi, "Dielectric relaxation in laser ablated polycrystalline ZrTiO[sub 4] thin films," *Journal of Applied Physics*, vol. 94, no. 8, Article ID 5135, 2003.

[37] R. Tripathi, A. Kumar, and T. P. Sinha, "Dielectric properties of CdS nanoparticles synthesized by soft chemical route," *Pramana—Journal of Physics*, vol. 72, no. 6, pp. 969–978, 2009.

[38] O. Oabi, A. Maaroufi, and B. Lucas, "Frequency electrical conductivity dependence and dielectric relaxation of ZnO–P2O5/Co composites," *Journal of Materials Science: Materials in Electronics*, vol. 29, no. 18, pp. 15902–15911, 2018.

[39] A. K. Jonscher, "The 'universal' dielectric response," *Nature*, vol. 267, no. 5613, pp. 673–679, 1977.